



HAL
open science

Human-induced greening of the northern extratropical land surface

Jiafu Mao, Aurélien Ribes, Binyan Yan, Xiaoying Shi, Peter Thornton, Roland Séférian, Philippe Ciais, Ranga Myneni, Hervé Douville, Shilong Piao, et al.

► **To cite this version:**

Jiafu Mao, Aurélien Ribes, Binyan Yan, Xiaoying Shi, Peter Thornton, et al.. Human-induced greening of the northern extratropical land surface. *Nature Climate Change*, 2016, 6 (10), pp.959-963. 10.1038/nclimate3056 . hal-02893073

HAL Id: hal-02893073

<https://hal.science/hal-02893073v1>

Submitted on 8 Oct 2024

HAL is a multi-disciplinary open access archive for the deposit and dissemination of scientific research documents, whether they are published or not. The documents may come from teaching and research institutions in France or abroad, or from public or private research centers.

L'archive ouverte pluridisciplinaire **HAL**, est destinée au dépôt et à la diffusion de documents scientifiques de niveau recherche, publiés ou non, émanant des établissements d'enseignement et de recherche français ou étrangers, des laboratoires publics ou privés.

Human-induced greening of the northern extratropical land surface

Jiafu Mao^{1†}, Aurélien Ribes², Binyan Yan³, Xiaoying Shi¹, Peter E. Thornton¹, Roland Séférian², Philippe Ciais⁴, Ranga B. Myneni⁵, Hervé Douville², Shilong Piao⁶, Zaichun Zhu⁶, Robert E. Dickinson³, Yongjiu Dai⁷, Daniel M. Ricciuto¹, Mingzhou Jin⁸, Forrest M. Hoffman⁹, Bin Wang^{10,11}, Mengtian Huang⁶, and Xu Lian⁶

- [1] Environmental Sciences Division and Climate Change Science Institute, Oak Ridge National Laboratory, Oak Ridge, TN, USA
- [2] Centre National de Recherches Météorologiques-Groupe d'Etude de l'Atmosphère Météorologique, Météo-France, Toulouse, France
- [3] Jackson School of Geosciences, the University of Texas, Austin, TX, USA
- [4] Laboratoire des Sciences du Climat et de l'Environnement, LSCE, 91191 Gif sur Yvette, France
- [5] Department of Earth and Environment, Boston University, Boston, MA 02215, USA
- [6] Sino-French Institute for Earth System Science, College of Urban and Environmental Sciences, Peking University, Beijing 100871, China
- [7] College of Global Change and Earth System Science, Beijing Normal University, Beijing, China
- [8] Department of Industrial and Systems Engineering, University of Tennessee, Knoxville, TN, USA
- [9] Computer Science and Mathematics Division and Climate Change Science Institute, Oak Ridge National Laboratory, Oak Ridge, TN 37831, USA
- [10] State Key Laboratory of Numerical Modeling for Atmospheric Sciences and Geophysical Fluid Dynamics, Institute of Atmospheric Physics, Beijing 100029, China
- [11] Center for Earth System Science, Tsinghua University, Beijing 100084, China

This manuscript has been authored by UT-Battelle, LLC under Contract No. DE-AC05-00OR22725 with the US Department of Energy. The United States Government retains and the publisher, by accepting the article for publication, acknowledges that the United States Government retains a non-exclusive, paid-up, irrevocable, world-wide license to publish or reproduce the published form of this manuscript, or allow others to do so, for United States Government purposes. The Department of Energy will provide public access to these results of federally sponsored research in accordance with the DOE Public Access Plan (<http://energy.gov/downloads/doe-public-access-plan>).

48 **Significant land greening in the northern-extratropical latitudes (NEL) has been**
49 **documented through satellite observations during the past three decades¹⁻⁵. This enhanced**
50 **vegetation growth has broad implications for surface energy, water and carbon budgets,**
51 **and ecosystem services across multiple scales⁶⁻⁸. Discernible human impacts on the Earth's**
52 **climate system have been revealed by using statistical frameworks of detection-attribution⁹⁻**
53 **¹¹. These impacts, however, were not previously identified on the NEL greening signal, due**
54 **to the lack of long-term observational records, possible bias of satellite data, different**
55 **algorithms used to calculate vegetation greenness, and the lack of suitable simulations from**
56 **coupled earth system models (ESMs). Here we have overcome these challenges in order to**
57 **attribute recent changes in NEL vegetation activity. We used two 30-year-long remote-**
58 **sensing-based Leaf Area Index (LAI) datasets^{12, 13}, simulations from 19 coupled ESMs with**
59 **interactive vegetation, and a formal detection and attribution algorithm^{14, 15}. Our findings**
60 **reveal that the observed greening record is consistent with an assumption of anthropogenic**
61 **forcings, where greenhouse gases play a dominant role, but is not consistent with**
62 **simulations that include only natural forcings and internal climate variability. These results**
63 **provide the first clear evidence of a discernible human fingerprint on physiological**
64 **vegetation changes other than phenology and range shifts¹¹.**

65
66 This study examines the growing season (GS) LAI over NEL (30°–75°N). The LAI is a
67 measurable biophysical parameter using satellite observation, an archived prognostic variable of
68 the Coupled Model Intercomparison Project Phase 5 (CMIP5) ESMs, and a direct indicator of the
69 leaf surface per unit ground area that exchanges energy, water, carbon dioxide and momentum
70 with the planetary boundary layer. We employed the recently published LAI3g dataset¹² and the
71 GEOLAND2 LAI data¹³, both of which were quality-controlled over the NEL region for the
72 1982–2011 period (Supplementary Information [SI] 1). We compared the observed changes of
73 LAI to simulated variations from multi-model results obtained from the CMIP5 archive (SI2 and
74 Table S1). These ensemble simulations comprise ALL, with historical anthropogenic and natural
75 forcings, GHG, with greenhouse gases forcing only, NAT, with natural forcing only, CTL, with
76 internal variability (IV) only, esmFixClim2, with CO₂ physiological effects, and esmFdbk2, with
77 greenhouse gases radiative effects. Beyond the standard comparison of time series and patterns of
78 trends, two methods were applied to detect and attribute changes in observed LAI, including a
79 formal “optimal fingerprint” analysis (Methods).

80
81 From 1982 to 2011, LAI3g, GEOLAND2 and their mean exhibited greening trends over NEL
82 vegetated area (85.3%, 69.5% and 80.6%, respectively), except across a narrow latitudinal band
83 over Canada and Alaska, and in a few spots over Eurasia (Figs. 1a–c). The largest positive
84 increase is observed in western Europe and eastern North America (NA) for both LAI products,
85 consistent with previous results¹⁻⁵. The multi-model ensemble-mean LAI changes under NAT
86 forcing had negative trends (browning) across vast areas of NA (51.9% of NA vegetated area)
87 and smaller positive trends over Eurasia (80.8% of Eurasia vegetated area) than in the averaged
88 satellite observations (86.8% of Eurasia vegetated area) (Fig. 1d). By contrast, the trend from the
89 ALL ensemble mean is closer to observations (Fig. 1e). The spatial distribution of observed LAI
90 trends was also well captured by the ensemble-mean GHG-only simulations (Fig. 1f). This
91 indicates that the combined anthropogenic effects, particularly the well-mixed greenhouse gases,
92 have contributed largely to widespread greening trends of NEL for the past three decades. Similar
93 results are obtained for the 1982–2011 period when different definitions of GS are chosen (Fig.
94 S1).

96 In NEL, the two remotely sensed LAI anomalies showed a large interannual variability
97 superimposed on an overall increasing trend (Fig. 2). These observed trends agree with those
98 found in the ALL and GHG ensembles, but were much larger than those simulated in the NAT
99 ensemble (Figs. 2, S2, and S3). Many observed values fall well outside the simulated 5th–95th
100 percentiles associated with individual NAT realizations, suggesting a clear inconsistency between
101 observations and this ensemble. The observations, however, are much more consistent with the
102 multi-model ensembles that are forced by the human-caused increases of greenhouse gases. The
103 comparison of the 1982–2011 observed trends (+0.143, +0.163 and +0.153 m²/m²/30yr for
104 LAI3g, GEOLAND2, and their average) with a set of 30-year segments from preindustrial control
105 simulations (Fig. 3a) confirms that the observed trends significantly exceed the range of values
106 expected from IV only under a stationary climate (± 0.066 m²/m²/30yr, p-value < 10⁻⁴) (SI3).
107 These observed trends also do not agree with trends in the NAT ensemble (Fig. 3b, p-value < 10⁻⁴)
108 ⁴), which, on average, is positive but much smaller (+0.017±0.054 m²/m²/30yr, or +0.017±0.066
109 m²/m²/30yr if the broadest IV estimate is used). In contrast, the observed trends are consistent
110 with those in the ALL ensemble (Fig. 3a, +0.133±0.089 m²/m²/30yr, p-value=0.64) as well as
111 GHG ensemble (Fig. 3b, +0.129±0.120 m²/m²/30yr, p-value=0.67). Similar results can be found
112 with different definitions of the GS (Fig. S4). According to the definitions used in IPCC AR4⁹,
113 this analysis allows us to attribute at least part of the observed LAI changes to human influence
114 because the trends are detectable, consistent with the expected response to all forcings, and
115 inconsistent with the expected response to natural forcings only (i.e., alternative, physically
116 plausible causes).

117
118 A more comprehensive and formal method used in IPCC AR5¹⁰ for attributing observed changes
119 involves an optimized regression of observations onto the expected response from models to one
120 or several external forcings (Methods). The main output from this type of analysis is the scaling
121 factor β , which scales the model's responses to best fit the observations. Assessing whether the
122 unexplained signal (i.e., the residuals of the regression) is consistent with IV is also a key
123 diagnosis in this method. This diagnosis is usually achieved using a residual consistency test
124 (RCT). We applied the detection and attribution (D&A) algorithm of refs. 14 and 15,
125 respectively, to the ALL and GHG-only temporal response patterns of 3-year mean LAI (as in
126 Fig. 2). We considered the average of all CMIP5 models in Multi1 (only one simulation from
127 each model) and the average of the models with larger ensembles in Multi3 (i.e., models with at
128 least three members) (Table S1). The observed LAI change over 1982–2011 is found to be
129 significant, as β scaling factors are significantly larger than 0 (Fig. 4). The 90% confidence
130 intervals of β include 1, which means that the observations are consistent with models, in terms of
131 the magnitude of the forced ALL and GHG-only responses. These two results are quite robust if
132 response patterns from individual models or individual observed datasets are considered.
133 However, the RCT is strongly rejected in most cases, even if all forcings are included, indicating
134 that the residuals of the fit are much larger than those expected from the simulated IV. In order to
135 deal with a possible underestimation of IV by ESMS, we tested the robustness of those key results
136 to several inflated IV assumptions (SI4). Detection was found to occur with all values of IV
137 variance that are consistent with observations, and even IV multiplied by a factor as large as 8,
138 which strongly reinforces confidence in our results.

139
140 With the human influence on recent evolution of NEL vegetation activity established, we are now
141 in a position to discuss the possible mechanisms behind those human influences (e.g., the impacts
142 of nitrogen deposition, land use/land cover change (LULCC), and the CO₂-induced physiological
143 vs. the GHG-induced climate effects) on LAI changes. We analyzed a smaller subset of CMIP5

144 ensemble models representing mechanisms of interest without using the D&A methodology
145 (Table S1). D&A techniques are not useful for discriminating between these forcings, as the
146 corresponding signals are usually too collinear over time, leading to a signal-to-noise ratio that is
147 too small. For the ALL simulations, models including the nitrogen cycle exhibited higher LAI
148 trends than those lacking explicit nitrogen cycles, reflecting in part a human influence from
149 increased nitrogen deposition (Figs. S7a and b). Consistent with the results of offline land surface
150 models including carbon-nitrogen dynamics (e.g., Fig. 4c in ref. 5), the difference seen in the
151 ESMs is particularly strong over eastern NA and eastern Asia, areas of known high levels of
152 human-caused nitrogen deposition¹⁶. The nitrogen-enabled models appear to capture observed
153 LAI trends in these regions (Fig. 1c). Slightly negative LAI trends observed over southwest NA,
154 western Canada, and spots of Eurasia seemed to correspond to the LULCC-induced vegetation
155 browning at the same locations (Figs. 1c and S7e). Nonetheless, the net LULCC-induced LAI
156 changes from CanESM2, the only model providing LULCC-only simulations, were quite small
157 (Fig. S9). CO₂ fertilization stimulated the vegetation growth over large areas of the NEL (83.8%
158 vegetated area) except in central NA (Fig. S7f). The response of modeled LAI to GHG-forced
159 climate change shows regions of decrease that coincide mainly with reduced precipitation and
160 regions of increase that coincide with regions of higher precipitation and warmer temperatures
161 (Figs. S7g and S8).

162
163 Previous work assessing modeled and observed LAI has focused on phenological variation,
164 interannual variability, and multiyear trends; spatiotemporal changes in LAI were attributed to
165 variation in climate drivers (mainly temperature and precipitation)¹⁷⁻²¹. This study adds to an
166 increasing body of evidence that NEL has experienced an enhancement of vegetation activity, as
167 reflected by increased trends in vegetation indices¹⁻⁵, aboveground vegetation biomass^{6,7}, and
168 terrestrial carbon fluxes²² during the satellite era. Our analysis goes beyond previous studies by
169 using D&A methods to establish that the trend of strengthened northern vegetation greening is
170 clearly distinguishable from both IV and the response to natural forcings alone. It can be
171 rigorously attributed, with high statistical confidence, to anthropogenic forcings, particularly to
172 rising atmospheric concentrations of greenhouse gases. As an attempt to decipher which
173 mechanisms are behind those trends, we further analyzed the contribution of nitrogen deposition,
174 LULCC, CO₂ fertilization and GHG-induced climate change to the NEL vegetation growth. This
175 provides potential leads to understanding the geographic structure of the vegetation response to
176 selected anthropogenic forcing agents.

177
178 An accurate quantification of the responses to individual human and natural drivers, however,
179 needs more research efforts, due to uncertainties associated with the ESMs, weaknesses of the
180 CMIP5 experimental design, and limitations in the observations. Relative to the observations, the
181 simulations with ALL and GHG forcings illustrated relatively weaker interannual variability of
182 vegetation growth (Figs. 2, S2 and S3). This discrepancy may arise from structural errors of the
183 land component in the ESMs (e.g., weak or no representation of vegetation mortality, disturbance
184 and successional dynamics)²³⁻²⁵. Since spatial and temporal patterns of vegetation growth are
185 tightly coupled with precipitation variability^{4, 17, 18}, the underestimation could also arise from the
186 reported underestimation of interannual precipitation variability in CMIP models over Northern
187 Hemisphere (NH) land^{26, 27}. Multi-model ensemble means can have persistent biases, such as
188 overprediction of growing season length due to advanced spring growth and delayed autumn
189 senescence in NH temperate ecosystems^{17, 28}. If such a phenological bias were changing steadily
190 over time, it could influence estimation of LAI trends reported here. We mitigate against this type
191 of bias by comparing our results for different seasonal periods. Since our results are consistent for

192 different definitions of GS (Figs. S1-S3), early and late season model biases, to the extent it is
193 present in our multi-model dataset, seem to be stationary in time. Understanding and ranking the
194 multiple reasons for deficiencies in CMIP5 simulations, however, remain extremely difficult,
195 given the lack of global LAI simulations with land surface models driven by common observed
196 environmental forcings. Such an obstacle should be overcome in the next phase of CMIP, which
197 will include an international intercomparison of the land surface components from the
198 participating ESMs²⁹. Long-term remote-sensing data are often contaminated by clouds and snow
199 cover and are impacted by the change of satellites³⁰. For example, the LAI3g dataset was likely
200 influenced in 1991 by the eruption of Mount Pinatubo and subsequent loss of orbit by NOAA 11,
201 seen particularly in the world's forests¹²; the merging of reflectance information from different
202 satellites during the pre- and post-2000 periods for both LAI3g and GEOLAND2 products has the
203 potential to cause inhomogeneity in the data^{12, 13}. These observational uncertainties, which are not
204 considered here, might artificially increase the observed interannual variability. Our sensitivity
205 tests, however, show that our key findings are robust to these issues, and the fingerprint patterns
206 assessed by the ALL and GHG ensembles can still be identified quantitatively in the relatively
207 short instrumental record.

208
209 Given the strong evidence provided here of historical human-induced greening in the northern
210 extratropics, society should consider both intended and unintended consequences of its
211 interactions with terrestrial ecosystems and the climate system.

212 213 **References**

- 214 1. Myneni, R. B., Keeling, C., Tucker, C., Asrar, G. and Nemani, R. Increased plant growth in the
215 northern high latitudes from 1981 to 1991. *Nature* **386**, 698–702 (1997).
- 216 2. Zhou, L. *et al.* Variations in northern vegetation activity inferred from satellite data of
217 vegetation index during 1981 to 1999. *J. Geophys. Res.: Atmos.* **106**, 20069–20083 (2001).
- 218 3. Lucht, W., *et al.* Climatic control of the high-latitude vegetation greening trend and Pinatubo
219 effect. *Science*. **296**, 1687–1689 (2002).
- 220 4. Mao, J. *et al.* Global latitudinal-asymmetric vegetation growth trends and their driving
221 mechanisms: 1982–2009. *Rem. Sens.* **5**, 1484–1497 (2013).
- 222 5. Buitenwerf, R., Rose, L. and Higgins, S. I. Three decades of multi-dimensional change in
223 global leaf phenology. *Nature Clim. Change* **5**, 364–368 (2015).
- 224 6. Pan, Y. *et al.* A large and persistent carbon sink in the world's forests. *Science* **333**, 988–993
225 (2011).
- 226 7. Liu, Y. Y. *et al.* Recent reversal in loss of global terrestrial biomass. *Nature Clim. Change* **5**,
227 470–474 (2015).
- 228 8. Ukkola, A. M. *et al.* Reduced streamflow in water-stressed climates consistent with CO₂
229 effects on vegetation. *Nature Clim. Change* advance online publication,
230 doi:10.1038/nclimate2831(2015).
- 231 9. Hegerl, G. C. *et al.* Understanding and attributing climate change. In: *Climate Change 2007:*
232 *The Physical Science Basis. Contribution of Working Group I to the Fourth Assessment*
233 *Report of the Intergovernmental Panel on Climate Change* (Cambridge Univ. Press, 2007).
- 234 10. Bindoff, N. L. *et al.* 2013: Detection and Attribution of Climate Change: from Global to
235 Regional. In: *Climate Change 2013: The Physical Science Basis. Contribution of Working*
236 *Group I to the Fifth Assessment Report of the Intergovernmental Panel on Climate Change*
237 (Cambridge Univ. Press, 2013).
- 238 11. Cramer, W., *et al.* Detection and attribution of observed impacts. In: *Climate Change 2014:*
239 *Impacts, Adaptation, and Vulnerability. Part A: Global and Sectoral Aspects. Contribution of*

- 240 Working Group II to the Fifth Assessment Report of the Intergovernmental Panel on Climate
241 Change (Cambridge University Press, 2014).
- 242 12. Zhu, Z. *et al.* Global data sets of vegetation leaf area index (LAI) 3g and fraction of
243 photosynthetically active radiation (FPAR) 3g derived from global inventory modeling and
244 mapping studies (GIMMS) normalized difference vegetation index (NDVI3g) for the period
245 1981 to 2011. *Rem. Sens.* **5**, 927–948 (2013).
- 246 13. Baret, F. *et al.* GEOV1: LAI and FAPAR essential climate variables and FCOVER global
247 time series capitalizing over existing products. part1: Principles of development and
248 production. *Rem. Sens. Environ.* **137**, 299–309 (2013).
- 249 14. Allen, M. and Stott, P. Estimating signal amplitudes in optimal fingerprinting, part I: theory.
250 *Clim. Dynam.* **21**, 477–491 (2003).
- 251 15. Ribes, A. Planton, S. and Terray, L. Application of regularised optimal fingerprinting to
252 attribution. part I: method, properties and idealised analysis. *Clim. Dynam.* **41**, 2817–2836
253 (2013).
- 254 16. Lamarque, J. F. *et al.* Multi-model mean nitrogen and sulfur deposition from the Atmospheric
255 Chemistry and Climate Model Intercomparison Project (ACCMIP): evaluation of historical
256 and projected future changes. *Atmos. Chem. Phys.* **13**, 7997–8018 (2013).
- 257 17. Anav, A. *et al.* Evaluation of land surface models in reproducing satellite derived leaf area
258 index over the high-latitude northern hemisphere. part II: earth system models. *Rem. Sens.* **5**,
259 3637–3661 (2013).
- 260 18. Mahowald, N. *et al.* Leaf Area Index in Earth System Models: evaluation and projections.
261 *Earth Syst. Dynam. Discuss.* **6**, 761–818, (2015).
- 262 19. Menzel, A. *et al.* European phenological response to climate change matches the warming
263 pattern. *Glob. Change Biol.* **12**, 1969–1976 (2006).
- 264 20. Zeng, F., Collatz, G., Pinzon, J. and Ivanoff, A. Evaluating and quantifying the climate-driven
265 interannual variability in Global Inventory Modeling and Mapping Studies (GIMMS)
266 Normalized Difference Vegetation Index (NDVI3g) at global scales. *Rem. Sens.* **5**, 3918–
267 3950 (2013).
- 268 21. Piao, S. *et al.* Evidence for a weakening relationship between interannual temperature
269 variability and northern vegetation activity. *Nature Commun.* **5**, 5018 (2014).
- 270 22. Anav, A. *et al.* Spatio-temporal patterns of terrestrial gross primary production: a review. *Rev.*
271 *Geophys.* **53**, 785–818 (2015).
- 272 23. McDowell, N.G. *et al.* Multi-scale predictions of massive conifer mortality due to chronic
273 temperature rise. *Nature Clim. Change* doi:10.1038/nclimate2873 (2015).
- 274 24. Di Vittorio, A.V. *et al.* From land use to land cover: restoring the afforestation signal in a
275 coupled integrated assessment–earth system model and the implications for CMIP5 RCP
276 simulations. *Biogeosciences*, **11**, 6435–6450 (2014).
- 277 25. Kunstler G. *et al.* Plant functional traits have globally consistent effects on competition.
278 *Nature* **529**, 204–207 (2016).
- 279 26. Zhang, X. *et al.* Detection of human influence on twentieth-century precipitation trends.
280 *Nature* **448**, 461–465 (2007).
- 281 27. Wu, P., Christidis, N. and Stott, P. Anthropogenic impact on Earth’s hydrological cycle.
282 *Nature Clim. Change* **3**, 807–810 (2013).
- 283 28. Keenan, T. F. *et al.* Net carbon uptake has increased through warming-induced changes in
284 temperate forest phenology. *Nature Clim. Change* **4**, 598–604 (2014).
- 285 29. Eyring, V., Bony, S., Meehl, G.A., Senior, C., Stevens, B., Stouffer, R.J. and Taylor, K.E.
286 Overview of the Coupled Model Intercomparison Project Phase 6 (CMIP6) experimental
287 design and organization. *Geosci. Model Dev. Discuss.* **8**, 10539–10583 (2015).

288 30. Pinzon, J. E. and Tucker, C. J. A non-stationary 1981-2012 AVHRR NDVI3g time series.
289 *Rem. Sens.* **6**, 6929–6960 (2014).

290
291 Correspondence and requests for materials should be addressed to maoj@ornl.gov.
292

293 **Acknowledgments**

294 This research is supported by the US Department of Energy (DOE), Office of Science, Biological
295 and Environmental Research. Oak Ridge National Laboratory is managed by UT-Battelle, LLC
296 for DOE under contract DE-AC05-00OR22725.

297 298 **Author contributions**

299 J.M. conceived the study. J.M., A.R., B.Y., X.S., P.T. and R.S. performed diagnostics and wrote
300 the text, with comments and edits from all authors.

301 302 **Additional information**

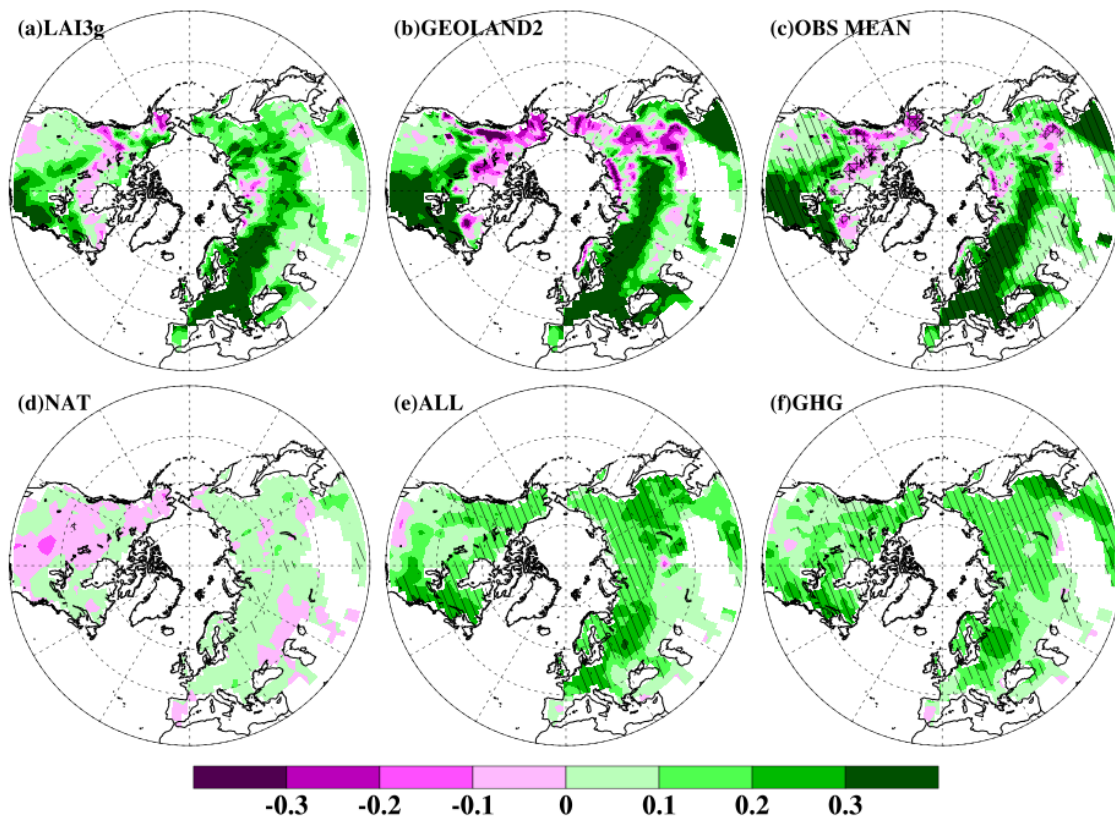
303 Supplementary information is available in the online version of the paper. Reprints and
304 permissions information is available online at www.nature.com/reprints.

305 306 **Competing financial interests**

307 The authors declare no competing financial interests.

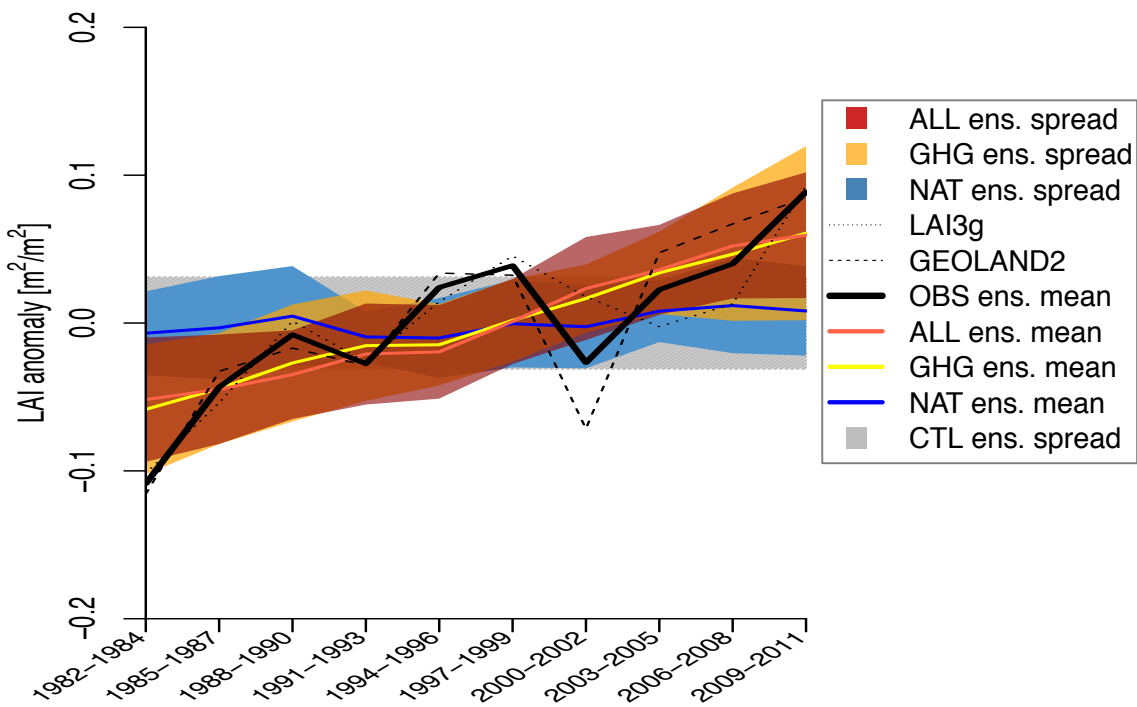
308 309 310 311 312 313 **Figures 1-4**

314



315
 316
 317
 318
 319
 320
 321
 322
 323
 324
 325
 326
 327
 328

Figure 1: Spatial distribution of LAI trends for 1982–2011. Spatial distribution of the linear trends in the growing season (April–October) LAI ($\text{m}^2/\text{m}^2/30\text{yr}$) in (a) LAI3g product, (b) GEOLAND2 product, (c) mean of LAI3g and GEOLAND2, (d) CMIP5 simulations with natural forcings alone (NAT), (e) CMIP5 simulations with anthropogenic and natural forcings (ALL), and (f) CMIP5 simulations with greenhouse gas forcings (GHG). The hatched area in (c) indicates that both satellite-based LAI datasets agree on the increasing trend of LAI, and the area with black crosses indicates that both satellite-based LAI datasets agree on the decreasing trend of LAI. The hatched area in (d)–(f) indicates that at least 90% of the simulation members agree on the increasing trend of LAI; the area with black crosses indicates that at least 90% of the simulation members agree on the decreasing trend of LAI.



329
 330
 331 **Figure 2: Observed and simulated 1982–2011 time series of LAI anomalies.** The 3-year mean
 332 growing season (April–October) LAI anomalies (m^2/m^2) over land of the northern-extratropical
 333 latitudes for both LAI3g and GEOLAND2 satellite-derived observations and CMIP5 simulations
 334 accounting for solely natural forcings (NAT) and greenhouse gas forcings (GHG) as well as
 335 CMIP5 simulations accounting for both anthropogenic and natural forcings (ALL). The ensemble
 336 mean for each set of forcings is given in blue, yellow, and red solid lines for NAT, GHG, and
 337 ALL, respectively. Individual satellite-derived observations are indicated with dashed black lines;
 338 the observational average is given with a bold solid black line. Blue, yellow, and red shading
 339 represent the 5%–95% confidence interval for NAT, GHG, and ALL ensembles, respectively
 340 (computed assuming a Gaussian distribution). The grey-hatched area represents the 5%–95%
 341 confidence interval for the range of variability for the centennial-long preindustrial unforced
 342 control simulations (CTL).

343
 344
 345
 346
 347
 348
 349
 350
 351
 352
 353
 354
 355
 356
 357

358
359
360
361
362
363
364
365
366
367
368
369
370
371
372
373
374
375
376
377
378
379
380
381
382
383
384
385
386
387
388

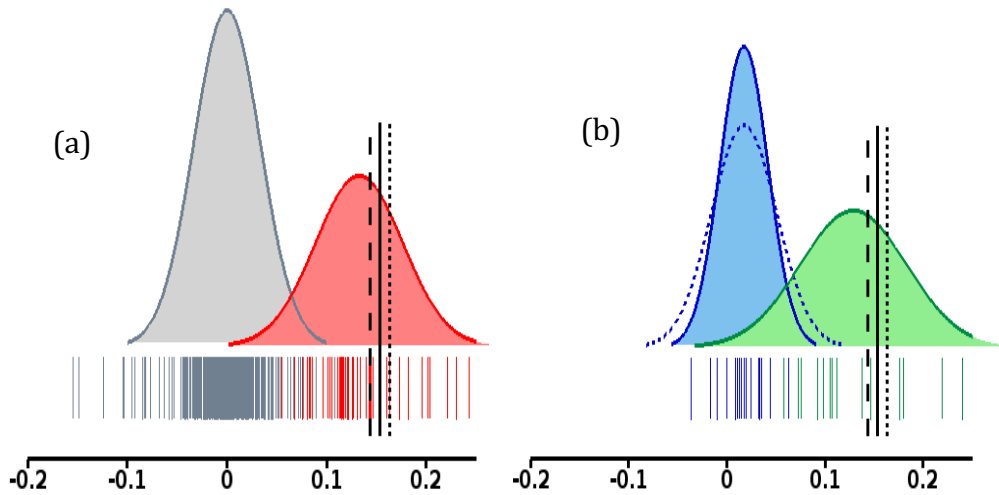
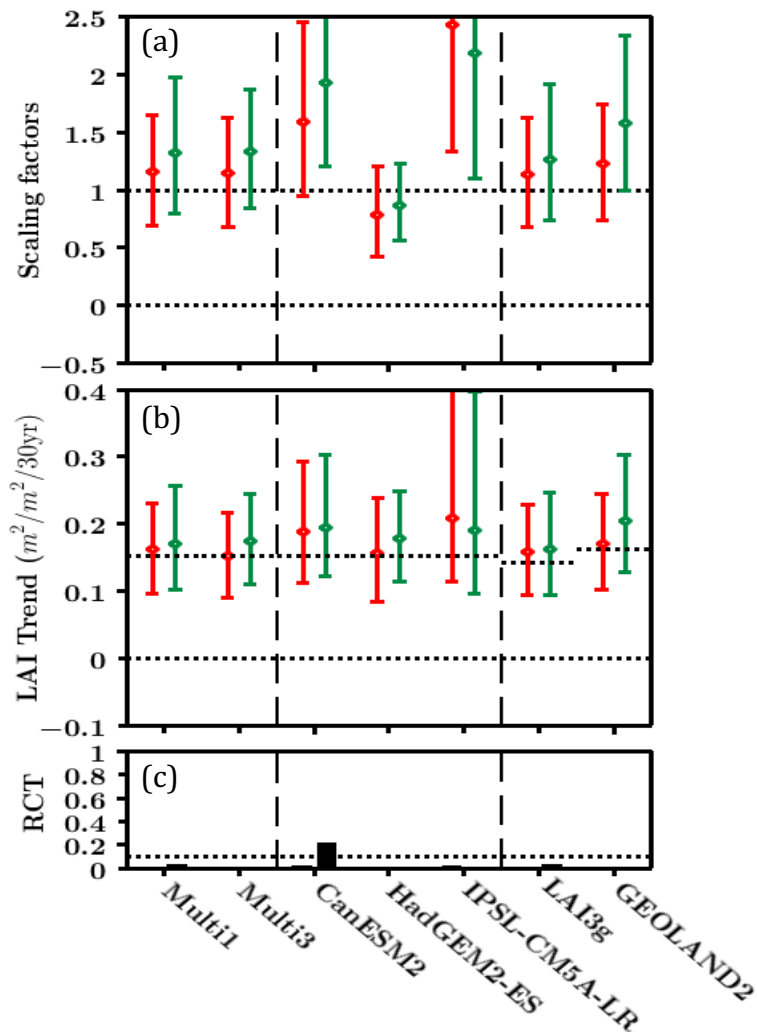


Figure 3: Parameterized frequency distributions of LAI 1982–2011 30-year-long trends.

Comparison of the observed trends ($\text{m}^2/\text{m}^2/30\text{yr}$) over land of the northern-extratropical latitudes from both LAI3g and GEOLAND2 satellite-derived observations, against the Gaussian-fitted probability density function (pdf) of simulated trends from CMIP5 simulations accounting for unforced preindustrial control variability (CTL, in grey), solely natural forcings (NAT, in blue) and greenhouse gas forcings (GHG, in green) as well as CMIP5 simulations accounting for both anthropogenic and natural forcings (ALL, in red). Individual satellite-derived observations are indicated with long and short vertical dashed black lines for LAI3g and GEOLAND2, respectively; the observational average is given with a bold solid black line. (a) Comparison between trends as estimated from satellite-derived products and as simulated from both individual 30-year segments taken from the CTL simulations and historical ALL simulations. (b) Comparison between trends as estimated from satellite-derived products and as simulated from NAT and GHG simulations. The dotted blue line, representing the pdf, corresponds to the NAT pdf but using a variance equal to that diagnosed from the CTL ensemble.



389

390 **Figure 4: Results from optimal D&A for 1982–2011 time series of LAI anomalies.**

391 The D&A analysis was performed over land of the northern-extratropical latitudes on ensemble-
 392 mean 1982–2011 time series of LAI anomalies. Response patterns were derived from CMIP5
 393 simulations accounting for both anthropogenic and natural forcings (ALL, in red), or greenhouse
 394 gas forcings only (GHG, in green), in a one-signal detection analysis. Observational average of
 395 LAI3g and GEOLAND2 was used as reference in the analysis. (a) Scaling factors (β —see text)
 396 best estimates and their 90% confidence intervals, (b) attributable trends over the 30-year-long
 397 time series, and (c) p-value of the residual consistency test (RCT). Results were obtained from a
 398 total least square (TLS) analysis using the multi-model mean or selected individual model
 399 responses. “Multi1” and “Multi3” refer to two different CMIP5 ensemble means (see text).
 400 Observational uncertainty was assessed using individual satellite-derived observations (LAI3g or
 401 GEOLAND2) regressed onto the “Multi1” response pattern.

402

403 **Methods**

404 **Detection and attribution.** Two distinct statistical approaches were used to detect and attribute
 405 the LAI changes in this study. The simple comparison of observed and simulated LAI trends (Fig.
 406 3) is based on a simple T-test, which is further discussed in the SI3. Then a more conventional
 407 D&A analysis is based on an optimal regression technique in which observations Y are regressed
 408 onto the expected response to historical forcing changes X^* (i.e., $Y = X^* \beta + \varepsilon$, where ε

409 denotes IV)^{14, 15, 31}. The scaling factors β are fitted using a total least square (TLS) approach,
410 where the expected response X^* is estimated from model-simulated responses X , which are also
411 contaminated by IV within the model simulation, $X = X^* + \epsilon x$. The model is fitted following
412 the method in ref. 15. The scaling factor β describes how the expected response has to be scaled
413 to best match observations. Conclusions in terms of the D&A are based on the best-estimate and
414 confidence interval on β . Attributable trends (i.e., the trends explained by the external forcing
415 under scrutiny)³² are derived by multiplying the model-simulated trend and the estimated scaling
416 factor $\hat{\beta}$. Similarly, upper and lower bounds of attributable trends are derived from the
417 corresponding upper and lower bounds of β . We applied these statistical methods to the NEL
418 average of 3-year mean LAI, as shown in Fig. 2. Natural internal variability is evaluated from
419 unforced control simulations from several CMIP5 climate models, and expected response patterns
420 are also taken from CMIP5 models (Table S1).

421

422 **References**

- 423 31. Allen, M. R. & Tett, S. F. Checking for model consistency in optimal fingerprinting. *Clim.*
424 *Dynam.* **15**, 419-434 (1999).
- 425 32. Stott, P. A., *et al.* Observational constraints on past attributable warming and predictions of
426 future global warming. *J. Clim.* **19**, 3055-3069 (2006).